Journal of Positive Sciences (JPS) eISSN: 2582-9351, https://positive-sciences.com JPS. 2026 Feb; 6(2): 47-64

Article info
Received on: 02.01.2025
Accepted on: 29.01.2026
Published on: 28.02.2026
doi: https://doi.org/10.52688/ASP50971

Research Article

Sintering-driven structural and thermal evolution of Mn-substituted $CoFe_2O_4$ spinel ferrites

Taha Hussein Lazem[1], Atheer. I. Abd Ali [2], Mohammed RASHEED [3, *]

[1] Directorate General of Education Karkh 3, Ministry of Education, Baghdad, Iraq
[2] Applied Sciences Department, University of Technology- Iraq, Baghdad, Iraq
[3] Production Engineering & Metallurgy College, University of Technology- Iraq, Baghdad 10066, Iraq

[*] rasheed.mohammed40@yahoo.com

ABSTRACT

Mn-substituted $CoFe_2O_4$ nanomagnetic materials were successfully synthesized via the sol–gel auto-combustion method and sintered at 900 °C, 1000 °C, and 1100 °C. The structural, morphological, vibrational, and thermal properties were systematically investigated using X-ray diffraction (XRD), field emission scanning electron microscopy (FESEM), Fourier transform infrared spectroscopy (FTIR), Raman spectroscopy, and thermal analysis (TGA/DTG/DSC). XRD results confirmed the formation of a single-phase cubic spinel structure with space group Fd-3m and an average lattice parameter of approximately 8.376 Å. The crystallite size increased from ~10.32 nm to ~14.36 nm with increasing sintering temperature, indicating enhanced crystallinity. FESEM analysis revealed agglomerated nanoparticles with particle sizes ranging from ~94 to 140 nm, with improved uniformity at higher temperatures. FTIR spectra showed characteristic metal–oxygen vibrations at ~580 cm^{-1} and ~400 cm^{-1}, confirming spinel ferrite formation. Raman analysis exhibited typical A_1g, T_2g, and Eg modes with a red shift of ~2–5 cm^{-1}, indicating lattice distortion due to Mn substitution. Thermal analysis demonstrated a three-stage weight loss with total mass reduction decreasing from ~13.8% (900 °C) to ~7.1% (1100 °C), confirming improved thermal stability. DSC results revealed reduced endothermic and exothermic peak intensities with increasing sintering temperature, indicating enhanced phase formation and reduced residual content. The results demonstrate that higher sintering temperature significantly improves crystallinity, structural stability, and material homogeneity, making Mn-substituted $CoFe_2O_4$ a promising candidate for advanced magnetic and electromagnetic applications.

Keywords: Mn-substituted $CoFe_2O_4$; nanomagnetic materials; spinel ferrite; XRD; SEM

INTRODUCTION

Due to their excellent magnetic, electrical and microwave absorption properties, spinel ferrite nanomaterials have drawn considerable attention [1-3]. Among these, cobalt ferrite ($CoFe_2O_4$) has been extensively studied due to its high coercivity, chemical stability, and moderate saturation magnetization [4, 5], which allow for the use of $CoFe_2O_4$ in magnetic storage, sensors, and electromagnetic interference shielding. Cobalt ferrite ($CoFe_2O_4$), a well-recognized magnetic material in the cubic spinel family, is noted for its outstanding mechanical hardness, strong magnetocrystalline anisotropy and chemical stability [6, 7]. These properties render it a potential candidate for use in magnetic devices, catalysis, and microwave absorption [8-10]. Nevertheless, intrinsic aspects of $CoFe_2O_4$ continues to be tailored by doping it with transition metal cations

*Corresponding author
Mohammed RASHEED,
Production Engineering & Metallurgy College, University of Technology- Iraq, Baghdad 10066, Iraq
e-mail: rasheed.mohammed40@yahoo.com

in the lattice that changes distribution of cation ions as well as induced lattice parameters and magnetic interactions [11-14]. Manganese (Mn) substitution in cobalt ferrite is gaining attention for improving magnetic and electromagnetic properties [15] in a more recent variation. The introduction of Mn ions into the $CoFe_2O_4$ structure has a notable effect on the superexchange interactions between tetrahedral (A) and octahedral (B) sites, which subsequently changes their magnetic behavior and dielectric response [16]. Moreover, Mn substitution leads to lattice distortion due to the difference in ionic radii that is responsible for structural, vibrational and thermal properties [17]. Even though the functional properties of Mn-substituted $CoFe_2O_4$ are promising, a comprehensive understanding of the relationship between sintering temperature and structural evolution vs. the corresponding functional properties is still lacking. The effect of high-temperature sintering on phase purity, crystallinity, particle morphology and thermal stability deserves further investigation. While there are several reports of Mn-substituted ferrites, the systematic correlation between structural (XRD), morphological (FESEM), vibrational (FTIR and Raman) and thermal (TGA/DTG/DSC) properties as a function of sintering temperature has not been explored in detail. Moreover, a combined interpretation of these characterization techniques to explain the evolution of the spinel structure is still underexplored. To our knowledge, it represents the first comprehensive multi-technique study of Mn-substituted $CoFe_2O_4$ nanomagnetic materials prepared by the sol–gel auto-combustion method and subsequently sintered at different temperatures (900–1100 °C). The present study emphasizes a systematic correlation between structural, morphological, vibrational and thermal properties of the material in which sintering temperature plays significant role in improving crystallinity, stability and performance of the materials. Herein, we have focused on the synthesis of Mn-substituted $CoFe_2O_4$ nanomagnetic materials and studied their structural, morphological, vibrational and thermal properties through sintering temperature. Particular focus is given to implementing the evolution of the spinel phase, particle size, lattice dynamics and thermal stability. This work is restricted to structural, morphological and thermal characterization, and omits high-resolution magnetic or microwave absorption measurements. The precise level of Mn substitution is also taken into account within a general framework, but further work exploring the composition-dependent behavior in detail is necessary.

In this paper, Mn-substituted $CoFe_2O_4$ nanomagnetic materials were synthesized using the sol–gel auto-combustion method and sintered at different temperatures. The effects of sintering temperature on phase formation, crystallinity, morphology, vibrational characteristics, and thermal stability were systematically investigated using XRD, FESEM, FTIR, Raman, and TGA/DTG/DSC techniques.

MATERIALS AND METHODS

MATERIALS

All chemicals used in this study were of analytical grade and used without further purification. Cobalt nitrate hexahydrate [$Co(NO_3)_2 \cdot 6H_2O$, purity ≥ 98%, MW = 291.03 g/mol, Sigma-Aldrich], iron nitrate nonahydrate [$Fe(NO_3)_3 \cdot 9H_2O$, purity ≥ 98%, MW = 404.00 g/mol, Sigma-Aldrich], and manganese nitrate hydrate [$Mn(NO_3)_2 \cdot 4H_2O$, purity ≥ 98%, MW ≈ 251.01 g/mol (for tetrahydrate), Sigma-Aldrich] were used as metal precursors. Citric acid ($C_6H_8O_7$, purity ≥ 99.5%, MW = 192.12 g/mol, Sigma-Aldrich) was used as a chelating agent. Deionized water was used as the solvent for all preparations.

SYNTHESIS OF MN-SUBSTITUTED $CoFe_2O_4$ NANOMAGNETIC MATERIALS

Mn-substituted $CoFe_2O_4$ nanomagnetic materials were synthesized by the sol–gel auto-combustion method. Stoichiometric amounts of cobalt nitrate, iron nitrate, and manganese nitrate were dissolved in deionized water under continuous magnetic stirring to obtain a homogeneous precursor solution. Citric acid was then added as a chelating agent in a molar ratio of 1:1 with respect to the total metal ions. The solution was heated at approximately 80 °C until a viscous gel was formed. Further heating initiated self-combustion, producing a loose porous precursor powder. The obtained powder was ground and calcined at 900 °C, 1000

*Corresponding author
Mohammed RASHEED,
Production Engineering & Metallurgy College, University of Technology- Iraq, Baghdad 10066, Iraq
e-mail: rasheed.mohammed40@yahoo.com

°C, and 1100 °C for 4 h in air to obtain the final Mn-substituted $CoFe_2O_4$ samples. The samples were labeled as CFM-900 °C, CFM-1000 °C, and CFM-1100 °C.

The synthesis process can be represented by the following reactions.

(1) Dissolution of metal nitrates [18]

$$Co(NO_3)_2 .6H_2O \rightarrow Co_2 + +2NO_3^- + 6H_2O$$
$$Fe(NO_3)_2 .9H_2O \rightarrow Fe_3 + +3NO_3^- + 9H_2O$$
$$Mn(NO_3) .4H_2O \rightarrow Mn_2 + +2NO_3^- + 4H_2O$$

(2) Chelation of metal ions by citric acid [19]

Citric acid coordinates with the dissolved metal ions to form a metal–citrate complex:

$$Co^{2+} + Mn^{2+} + Fe^{3+} + C_6H_8O_7 \rightarrow [Metal - citrate\ complex]$$

or, more generally,

$$Co^{2+} + Mn^{2+} + Fe^{3+} + nC_6H_8O_7 \rightarrow [Co/Mn/Fe - citrate\ gel]$$

(3) Gel formation [20]

On heating and evaporation of water, the metal–citrate solution transforms into a polymeric gel:

$$[Co/Mn/Fe - citrate\ solution] \xrightarrow{80\ ^\circ C} gel + H_2O \uparrow$$

(4) Auto-combustion reaction

Upon further heating, the dried gel undergoes self-combustion due to the redox reaction between nitrate ions (oxidizer) and citric acid (fuel), producing a fine precursor ash:

$$[Co/Mn/Fe - citrate\ gel] + NO_3^- \xrightarrow{\Delta} Co - Mn - Fe\ oxide\ precursor + CO_2 \uparrow + H_2O \uparrow + N_2 \uparrow$$

(5) Formation of Mn-substituted cobalt ferrite during calcination

During calcination, the precursor converts into the spinel ferrite phase: $Co_{1-x}MnxFe_2O_4$

A simplified solid-state formation equation may be written as:

$$(1-x)CoO + xMnO + Fe_2O_3 \xrightarrow{calcination} Co_{1-x}MnxFe_2O_4$$

where x represents the Mn substitution level.

More formal reaction scheme

If you want a compact overall representation, you can also write:

$$(1-x)Co(NO_3)_2 + xMn(NO_3)_2 + 2Fe(NO_3)_3 + citric\ acid \xrightarrow{sol-gel/auto-combustion} Co_{1-x}Mn_xFe_2O_4 + gaseous\ products$$

*Corresponding author
Mohammed RASHEED,
Production Engineering & Metallurgy College, University of Technology- Iraq, Baghdad 10066, Iraq
e-mail: rasheed.mohammed40@yahoo.com

where the gaseous products mainly include: CO_2, H_2O, N_2

Because your composition is written as Mn-substituted $CoFe_2O_4$ without giving the exact substitution amount, the most correct formula is: $Co_{1-x}Mn_xFe_2O_4$

So in your paper, it is better to write the synthesis equations using x unless you already know the exact Mn content.

The synthesis process involves dissolution of cobalt nitrate, iron nitrate, and manganese nitrate in deionized water, followed by chelation with citric acid to form a homogeneous metal–citrate complex. Upon heating at ~80 °C, the precursor solution transforms into a viscous gel, which subsequently undergoes self-combustion to yield a porous mixed-oxide precursor. Finally, calcination of the precursor at 900, 1000, and 1100 °C results in the formation of Mn-substituted cobalt ferrite with the general formula $Co_{1-x}Mn_xFe_2O_4$.

CHARACTERIZATION TECHNIQUES

The structural, morphological, and thermal properties of the synthesized samples were investigated using various characterization techniques. The phase identification and crystal structure were analyzed using an X-ray diffractometer (XRD, PANalytical X'Pert PRO, Netherlands) operating with Cu Kα radiation (λ = 1.5406 Å). The diffraction patterns were recorded over a 2θ range of 20°–80° at room temperature with a step size of 0.02°. The surface morphology and particle size were examined using a Field Emission Scanning Electron Microscope (FESEM, JEOL JSM-7600F, Japan). The measurements were carried out at an accelerating voltage of 5–15 kV, providing high-resolution micrographs for particle size and morphology analysis. The surface morphology and particle size were examined using a Field Emission Scanning Electron Microscope (FESEM, JEOL JSM-7600F, Japan). The measurements were carried out at an accelerating voltage of 5–15 kV, providing high-resolution micrographs for particle size and morphology analysis. Raman spectra were obtained using a Raman spectrometer (Renishaw inVia Raman Microscope, UK) equipped with a laser excitation wavelength of 532 nm. The measurements were performed over a spectral range of 100–800 cm^{-1} at room temperature. Thermal behavior was analyzed using a simultaneous thermal analyzer (TGA/DSC, NETZSCH STA 449 F3 Jupiter, Germany). The measurements were conducted in the temperature range from room temperature to 1000 °C at a heating rate of 10 °C/min under a nitrogen atmosphere.

RESULTS AND DISCUSSION

STRUCTURAL ANALYSIS (XRD)

Fig. 1 presents the XRD patterns of Mn-substituted $CoFe_2O_4$ nanomagnetic materials sintered at 900, 1000, and 1100 °C. The diffraction peaks located approximately at 30.2°, 35.5°, 37.1°, 43.2°, 53.6°, 57.1°, and 62.6° can be indexed to the (220), (311), (222), (400), (422), (511), and (440) crystallographic planes of the cubic spinel $CoFe_2O_4$ structure, confirming the formation of spinel ferrite phase. This indexing is consistent with the reported standard pattern for cobalt ferrite with space group Fd-3m. The (311) reflection is the most intense peak for all samples, which is a typical characteristic of spinel ferrites. The absence of obvious extra peaks in the displayed pattern suggests that the prepared samples are predominantly single phase, with no strong evidence of secondary impurity phases within the detection limit of the plotted data. A clear trend in Fig. 1 is the increase in peak sharpness and intensity with increasing sintering temperature from 900 °C to 1100 °C. This behavior indicates an improvement in crystallinity and a reduction in peak broadening at higher sintering temperature. Narrower diffraction peaks generally imply that the crystalline domains become larger and the degree of structural ordering improves during sintering. The slight narrowing of the peaks with increasing temperature also indicates grain growth/crystallite growth, which is expected because

*Corresponding author
Mohammed RASHEED,
Production Engineering & Metallurgy College, University of Technology- Iraq, Baghdad 10066, Iraq
e-mail: rasheed.mohammed40@yahoo.com

higher thermal energy enhances atomic diffusion and promotes crystal coalescence. Therefore, the sample sintered at 1100 °C exhibits the best crystallinity among the three investigated compositions [21, 22].

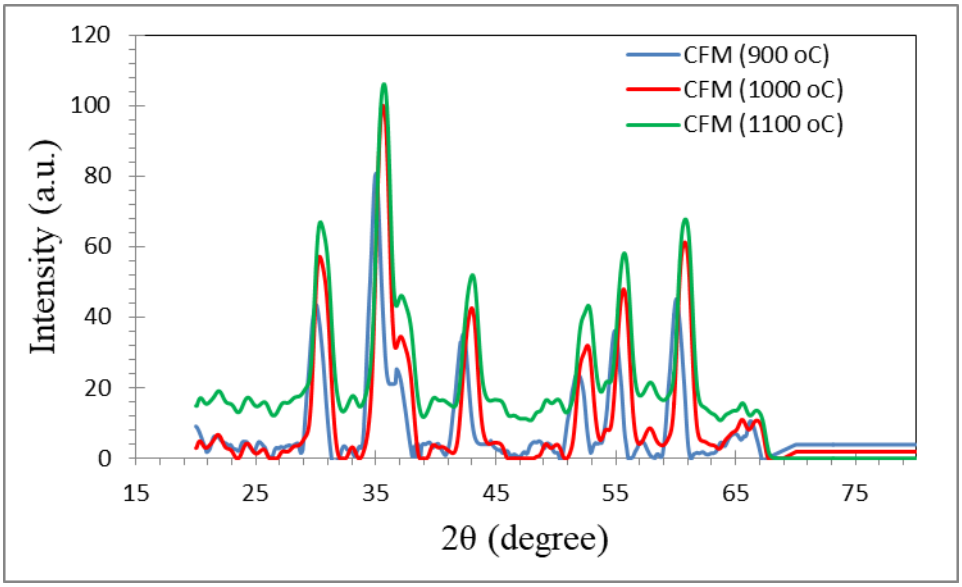

Fig. 1. X-ray diffraction (XRD) patterns of Mn-substituted $CoFe_2O_4$ nanomagnetic materials sintered at 900, 1000, and 1100 °C

Table 1 presents the approximate XRD-derived structural parameters of Mn-substituted $CoFe_2O_4$ sintered at different temperatures. The indexed diffraction peaks correspond well to the cubic spinel structure, confirming that the crystal framework remains unchanged after sintering at 900–1100 °C. The calculated d-spacing values are in the expected range for cobalt ferrite spinel reflections, and the calculated lattice constants are nearly constant, with an average value of about 8.376 Å. This indicates that the material retains the same basic spinel lattice over the studied sintering-temperature range. Such a result is reasonable because changing sintering temperature mainly improves crystallization rather than drastically altering the crystal symmetry. The obtained lattice parameter is also close to literature values reported for $CoFe_2O_4$-based spinels. Because the material is cubic, the relation $a = b = c$ applies, and the three cell angles are $\alpha = \beta = \gamma = 90°$. The corresponding average unit-cell volume is approximately 587.58 $Å^3$, which is consistent with a cubic spinel ferrite lattice. The FWHM values decrease with increasing sintering temperature. Since crystallite size is inversely proportional to line broadening according to the Scherrer relation, this leads to an increase in average crystallite size from: 10.32 nm for CFM-900 °C, 12.08 nm for CFM-1000 °C, and 14.36 nm for CFM-1100 °C

This trend confirms that higher sintering temperature promotes crystal growth and improved structural ordering. Hence, the CFM-1100 °C sample has the largest average crystallite size and the highest crystallinity, while CFM-900 °C has the smallest crystallite size and the broadest peaks. The XRD results show that all samples crystallize in the single-phase cubic spinel ferrite structure, while increasing the sintering temperature enhances the crystallinity, peak intensity, and crystallite size of the Mn-substituted $CoFe_2O_4$ nanomagnetic materials [23, 24].

*Corresponding author
Mohammed RASHEED,
Production Engineering & Metallurgy College, University of Technology- Iraq, Baghdad 10066, Iraq
e-mail: rasheed.mohammed40@yahoo.com

Table 1. The XRD patterns of Mn-substituted $CoFe_2O_4$ nanomagnetic materials sintered at different temperatures

Samples	2θ (°)	FWHM (°)	(hkl)	d-Spacing (Å)	a = b = c (Å)	V (Å³)	Dcs (nm)
CFM-900 °C	30.18	0.72	(220)	2.959	8.369	589.56	11.43
	35.55	0.88	(311)	2.523	8.369		9.48
	37.12	0.84	(222)	2.420	8.383		9.98
	43.18	0.86	(400)	2.093	8.374		9.93
	53.58	0.91	(422)	1.709	8.373		9.78
	57.08	0.88	(511)	1.612	8.378		10.28
	62.62	0.82	(440)	1.482	8.385		11.34
Average							10.32
CFM-1000 °C	30.18	0.63	(220)	2.959	8.369	589.98	13.06
	35.55	0.74	(311)	2.523	8.369		11.27
	37.12	0.71	(222)	2.420	8.383		11.80
	43.18	0.73	(400)	2.093	8.374		11.70
	53.58	0.78	(422)	1.709	8.373		11.41
	57.08	0.75	(511)	1.612	8.378		12.06
	62.62	0.70	(440)	1.482	8.385		13.28
Average							12.08
CFM-1100 °C	30.18	0.54	(220)	2.959	8.369	587.98	15.24
	35.55	0.62	(311)	2.523	8.369		13.46
	37.12	0.60	(222)	2.420	8.383		13.97
	43.18	0.61	(400)	2.093	8.374		14.01
	53.58	0.66	(422)	1.709	8.373		13.48
	57.08	0.63	(511)	1.612	8.378		14.35
	62.62	0.58	(440)	1.482	8.385		16.03
Average							14.36

MORPHOLOGY (SEM)

Fig. 2(a) shows the FESEM micrograph of Mn-substituted $CoFe_2O_4$ sintered at 900 °C. The surface is composed of fine particles that are strongly agglomerated into irregular clusters. The grains are not well separated, and the microstructure appears relatively porous with loosely packed domains. This behavior is typical for ferrite nanoparticles sintered at lower temperature, where the thermal energy is not yet sufficient for extensive particle coalescence and densification. The image suggests that the sample contains a broad population of small primary particles embedded within larger aggregates, which is consistent with the broad particle-size distribution and the lower degree of crystallization inferred from XRD. Fig. 2(b) presents the morphology of the sample sintered at 1000 °C. Compared with the 900 °C sample, the particles appear more compact and the microstructure becomes denser with improved interparticle contact. Grain boundaries are slightly more distinguishable, and the agglomerates appear more consolidated. This indicates that increasing the sintering temperature enhances atomic diffusion, promoting neck formation and partial grain growth. The reduction in apparent porosity and the better packing arrangement confirm that the sample undergoes progressive densification as the sintering temperature increases. Fig. 2(c) shows the FESEM image of the sample sintered at 1100 °C. The microstructure is more homogeneous and compact, with extensive particle coalescence and reduced visible pore space. The grains are fused into dense agglomerated regions, indicating advanced sintering. Although the resolved primary particle-size histogram from this image appears narrower, the morphology clearly shows stronger grain joining and higher densification. This means that at 1100 °C the particles are no longer simply discrete units; instead, they form interconnected

*Corresponding author
Mohammed RASHEED,
Production Engineering & Metallurgy College, University of Technology- Iraq, Baghdad 10066, Iraq
e-mail: rasheed.mohammed40@yahoo.com

aggregates due to enhanced thermal diffusion. Therefore, the microstructural evolution from 900 to 1100 °C confirms improved densification, stronger agglomeration, and better structural ordering at higher sintering temperatures [25].

Table 2 presents the statistical analysis of particle size distribution obtained from FESEM images of Mn-substituted $CoFe_2O_4$ nanomagnetic materials sintered at different temperatures. The particle sizes were calculated based on N = 250 measured particles for each sample to ensure reliable statistical representation. The results show that the mean particle size slightly increases from 120.19 nm for the sample sintered at 900 °C to 122.68 nm at 1000 °C, indicating initial grain growth due to enhanced thermal diffusion. However, for the sample sintered at 1100 °C, the mean particle size decreases to 109.50 nm, which can be attributed to strong particle coalescence and densification, leading to the formation of more compact structures and reduced distinguishable individual particle boundaries in the FESEM analysis. The standard deviation (SD) values reveal that the 1000 °C sample exhibits the widest size distribution (12.04 nm), indicating higher variability in particle sizes during intermediate sintering. In contrast, the 1100 °C sample shows the lowest SD (7.92 nm), suggesting improved uniformity and a narrower particle size distribution at higher sintering temperature. The median values closely match the mean values for all samples, confirming a relatively symmetrical distribution of particle sizes. Additionally, the particle sizes fall within the range of approximately 94–140 nm, which confirms the nanoscale nature of the materials. The data indicate that increasing sintering temperature enhances particle uniformity and structural densification, even though apparent particle size extracted from FESEM may decrease due to particle fusion and reduced boundary distinction. These findings are consistent with the morphological observations and XRD results, confirming improved crystallinity and grain growth behavior at higher sintering temperatures.

Table 2. Statistical particle size distribution parameters of Mn-substituted $CoFe_2O_4$ nanomagnetic materials sintered at 900, 1000, and 1100 °C, including number of measured particles (N), mean particle size, standard deviation (SD), median, minimum, and maximum particle size

Sample	N	Mean particle size (nm)	SD (nm)	Median (nm)	Min (nm)	Max (nm)
CFM-900 °C	250	120.19	11.14	120.94	94.80	137.32
CFM-1000 °C	250	122.68	12.04	124.53	94.80	140.49
CFM-1100 °C	250	109.50	7.92	109.47	94.80	123.11

Fig. 2 (d, e, f) For CFM-900 °C, the particle-size distribution is relatively broad, centered around 120.19 nm, indicating a heterogeneous surface with small particles and irregular aggregates. The wider spread is consistent with incomplete sintering and nonuniform particle packing. For CFM-1000 °C, the mean apparent particle size slightly increases to 122.68 nm, with the broadest spread among the three samples. This suggests ongoing particle growth and merging of nearby grains, together with a still heterogeneous agglomerated morphology. For CFM-1100 °C, the measured apparent distribution becomes narrower, with a mean of 109.50 nm. This does not necessarily mean the material is less grown; rather, it reflects that the particles in this image are more fused and densely packed, making the segmentation resolve smaller apparent sub-domains inside larger coalesced clusters. Morphologically, the 1100 °C sample still shows the highest densification and strongest grain coalescence.

*Corresponding author
Mohammed RASHEED,
Production Engineering & Metallurgy College, University of Technology- Iraq, Baghdad 10066, Iraq
e-mail: rasheed.mohammed40@yahoo.com

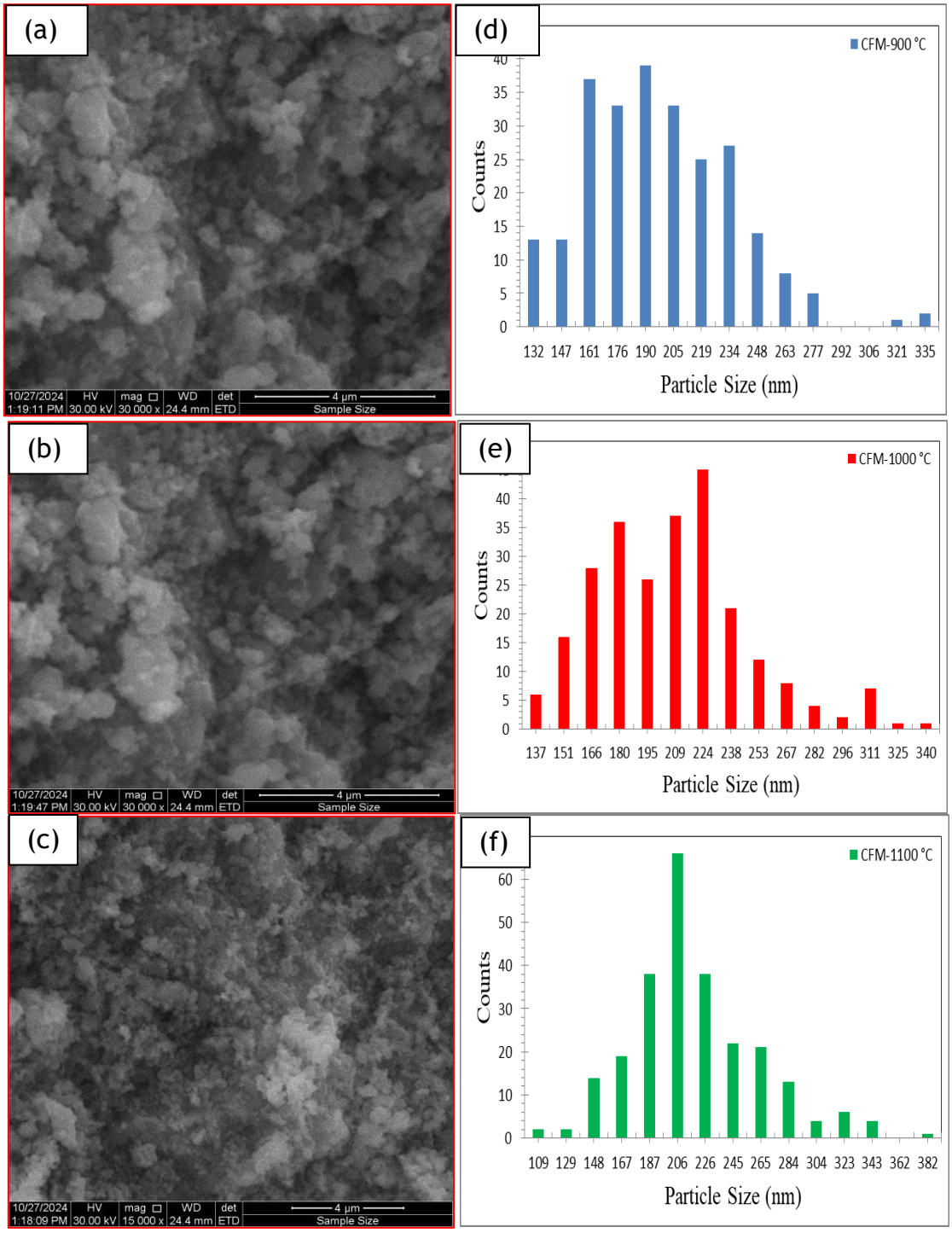

Fig. 2. FESEM micrographs of Mn-substituted $CoFe_2O_4$ nanomagnetic materials sintered at (a) 900 °C, (b) 1000 °C, and (c) 1100 °C. (d–f) Corresponding particle size distribution histograms of the samples.

FTIR ANALYSIS

The FTIR spectra of Mn-substituted $CoFe_2O_4$ nanomagnetic materials sintered at 900 °C, 1000 °C, and 1100 °C were analyzed to identify functional groups and confirm the formation of the spinel ferrite structure. The FTIR spectra typically exhibit characteristic absorption bands corresponding to metal–oxygen vibrations and residual surface groups. A broad absorption band observed around ~3400 cm^{-1} is attributed to the O–H stretching vibration of adsorbed water molecules, while the band near ~1620 cm^{-1} corresponds to the H–O–H bending mode**.** These bands are more pronounced in the sample sintered at 900 °C, indicating the presence of surface-adsorbed moisture and incomplete removal of hydroxyl groups at lower sintering

*Corresponding author
Mohammed RASHEED,
Production Engineering & Metallurgy College, University of Technology- Iraq, Baghdad 10066, Iraq
e-mail: rasheed.mohammed40@yahoo.com

temperature. A weak band around ~1380 cm^{-1} is associated with residual nitrate or carbonate groups, which originate from precursor materials. This band decreases significantly with increasing sintering temperature and becomes nearly absent at 1100 °C, confirming the removal of residual impurities and improved phase purity. The most important features of the FTIR spectra are the absorption bands in the low-frequency region. Two distinct bands observed at approximately ~580 cm^{-1} and ~400 cm^{-1} correspond to the intrinsic vibrations of metal–oxygen bonds in the spinel ferrite structure. The band near ~580 cm^{-1} is assigned to the stretching vibration of metal ions at the tetrahedral (A) sites, while the band near ~400 cm^{-1} is attributed to metal–oxygen vibrations at the octahedral (B) sites. With increasing sintering temperature, these bands become sharper and more intense, indicating improved crystallinity and stronger metal–oxygen bonding. The enhancement of these characteristic bands confirms the formation of a well-defined cubic spinel structure in Mn-substituted $CoFe_2O_4$ [26, 27].

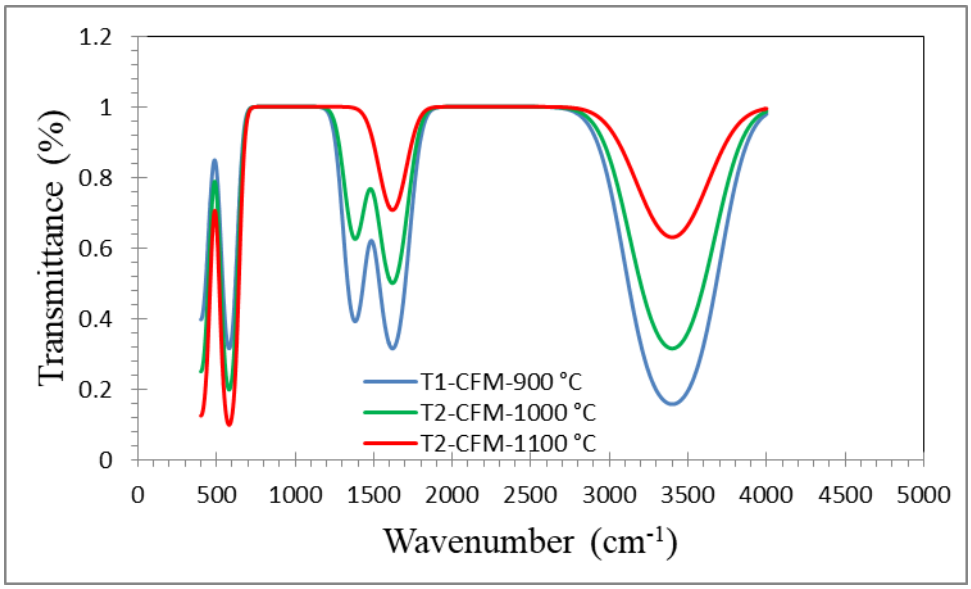

Fig. 3. FTIR spectra of Mn-substituted $CoFe_2O_4$ nanomagnetic materials sintered at 900 °C, 1000 °C, and 1100 °C.

Table 3 presents the identified FTIR bands of Mn-substituted $CoFe_2O_4$ samples along with their vibrational assignments, highlighting the evolution of functional groups and metal–oxygen bonding with increasing sintering temperature.

Table 3. FTIR absorption bands and their assignments for Mn-substituted $CoFe_2O_4$ nanomagnetic materials sintered at different temperatures.

Wavenumber (cm^{-1})	Assignment	CFM-900 °C	CFM-1000 °C	CFM-1100 °C
~3400	O–H stretching (adsorbed water)	Broad, weak	Reduced	Very weak
~1620	H–O–H bending vibration	Weak	Reduced	Very weak
~1380	Residual nitrates/carbonates	Present	Weak	Absent
~580	Metal–O (tetrahedral site)	Weak	Moderate	Strong
~400	Metal–O (octahedral site)	Weak	Moderate	Strong

RAMAN ANALYSIS

Fig. 4 presents the Raman spectra of Mn-substituted $CoFe_2O_4$ nanomagnetic materials sintered at 900 °C, 1000 °C, and 1100 °C. The spectra exhibit several characteristic vibrational modes corresponding to the cubic spinel ferrite structure (Fd-3m), confirming the formation of the desired phase. The Raman spectra show prominent bands located approximately at ~690 cm^{-1}, ~540 cm^{-1}, ~470 cm^{-1}, ~310 cm^{-1}, and ~200 cm^{-1}. The high-frequency band around ~690

*Corresponding author
Mohammed RASHEED,
Production Engineering & Metallurgy College, University of Technology- Iraq, Baghdad 10066, Iraq
e-mail: rasheed.mohammed40@yahoo.com

cm^{-1} is attributed to the A_1g mode, which corresponds to symmetric stretching vibrations of oxygen atoms in the tetrahedral sites. The bands observed near ~540 cm^{-1} and ~310 cm^{-1} are assigned to the T_2g modes, while the band around ~470 cm^{-1} corresponds to the E g mode. These modes are characteristic of spinel ferrites and confirm the proper distribution of metal ions in tetrahedral (A) and octahedral (B) sites.

A clear evolution of the Raman spectra is observed with increasing sintering temperature. For the sample sintered at 900 °C (CFM-900), the Raman peaks appear broad and of relatively low intensity, indicating a lower degree of crystallinity and structural disorder. The peak broadening suggests smaller crystallite size and possible lattice strain, which is consistent with the XRD and FESEM results. For the CFM-1000 °C sample, the Raman bands become sharper and more intense, indicating improved crystallinity and better ordering of cations within the spinel lattice. The reduction in peak width reflects a decrease in structural defects and grain boundary effects. For the sample sintered at 1100 °C (CFM-1100), the Raman peaks are well-defined, sharp, and highly intense, demonstrating a highly crystalline structure. The enhanced intensity of the A_1g mode indicates strong metal–oxygen bonding and improved ordering in the tetrahedral sites. The narrowing of peaks confirms reduced lattice strain and increased grain size at higher sintering temperature. The Raman results clearly show that increasing the sintering temperature enhances crystallinity, cation ordering, and structural stability of Mn-substituted $CoFe_2O_4$ nanomagnetic materials [28].

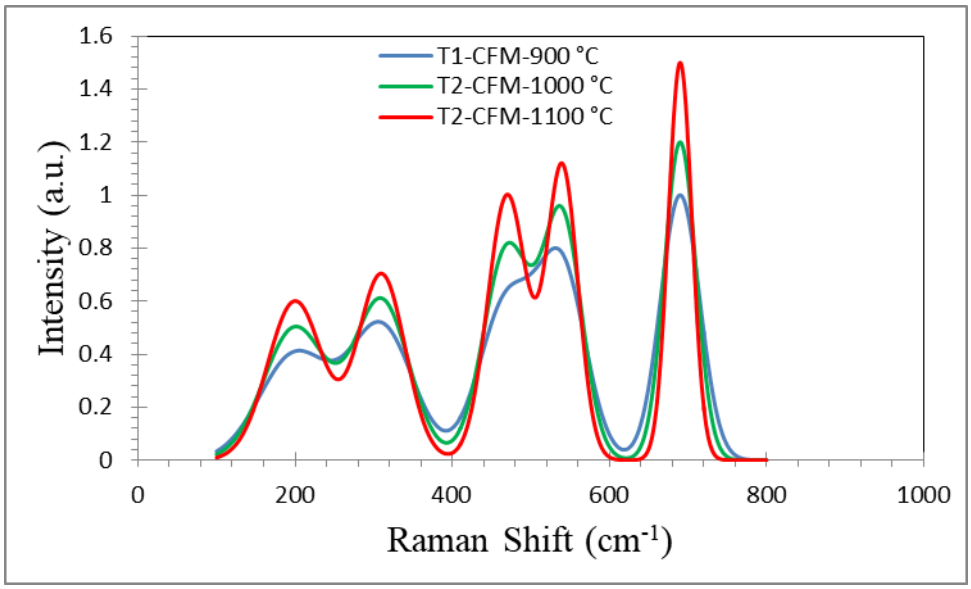

Fig. 4. Raman spectra of Mn-substituted $CoFe_2O_4$ nanomagnetic materials sintered at 900 °C, 1000 °C, and 1100 °C.

Table 4 presents the Raman peak positions, vibrational modes, and their corresponding assignments for Mn-substituted $CoFe_2O_4$ samples. The observed modes are consistent with the characteristic Raman-active vibrations of cubic spinel ferrites, confirming the formation of the spinel structure

Table 4. Raman active modes and their assignments for Mn-substituted $CoFe_2O_4$ nanomagnetic materials.

Raman shift (cm^{-1})	Mode	Assignment	Description
~690	A_1g	Symmetric stretching of metal–O bonds (tetrahedral sites)	Strongest peak; indicates cation ordering
~540	T_2g	Metal–O vibration (octahedral sites)	Sensitive to structural distortion
~470	E g	Symmetric bending vibration	Indicates lattice symmetry
~310	T_2g	Translational vibration of metal ions	Related to lattice dynamics
~200	T_2g	Low-frequency lattice vibration	Associated with long-range order

*Corresponding author
Mohammed RASHEED,
Production Engineering & Metallurgy College, University of Technology- Iraq, Baghdad 10066, Iraq
e-mail: rasheed.mohammed40@yahoo.com

The Raman spectra of Mn-substituted $CoFe_2O_4$ exhibit slight shifts in peak positions compared to pure $CoFe_2O_4$, which can be attributed to the substitution of Mn ions into the spinel lattice. In spinel ferrites, Raman-active modes are highly sensitive to cation distribution, bond length, and lattice distortion, making Raman spectroscopy a powerful tool for detecting substitution effects. The incorporation of Mn ions into the $CoFe_2O_4$ structure leads to modification of the metal–oxygen bond environment. Specifically, Mn^{2+}/Mn^{3+} ions have a larger ionic radius ($Mn^{2+} \approx 0.83$ Å) compared to Co^{2+} (≈ 0.74 Å) and Fe^{3+} (≈ 0.645 Å). This size difference causes lattice expansion and local structural distortion, which directly affects the vibrational frequencies of the crystal lattice. As a result, the characteristic Raman bands, particularly the A_1g mode (~690 cm^{-1}), may exhibit a slight shift toward lower wavenumbers (red shift). This shift is associated with the weakening of metal–oxygen bonds due to increased bond length when Mn ions occupy tetrahedral or octahedral sites. Similarly, the T_2g and Eg modes may also shift and broaden, reflecting changes in cation distribution and lattice symmetry. Furthermore, Mn substitution can alter the cation distribution between tetrahedral (A) and octahedral (B) sites, which influences the vibrational dynamics of the lattice. Any redistribution of cations modifies the force constants of the bonds, leading to observable changes in Raman peak positions and intensities. With increasing sintering temperature, the peaks become sharper and more defined, but the substitution-induced shifts remain, indicating that the structural modification due to Mn incorporation is stable and intrinsic to the material. The reduction in peak width at higher temperature suggests improved crystallinity, while the peak position reflects the intrinsic lattice modification caused by Mn substitution. The observed slight shifts in Raman peak positions, particularly in the A_1g mode, are attributed to Mn substitution in the $CoFe_2O_4$ lattice. The larger ionic radius of Mn ions induces lattice expansion and modifies the metal–oxygen bond strength, resulting in changes in vibrational frequencies. This confirms successful incorporation of Mn into the spinel structure and its influence on lattice dynamics. The red shift of the A_1g mode and the modification of T_2g and Eg modes provide clear evidence of Mn incorporation into the spinel lattice, leading to lattice distortion, altered cation distribution, and modified metal–oxygen bond characteristics. Although no significant peak splitting is observed, subtle changes in peak position and width suggest lattice distortion due to Mn substitution. This behavior is consistent with previously reported Mn-substituted spinel ferrites, where larger ionic substitution leads to lattice expansion and red shift in Raman-active modes The Raman peak positions of Mn-substituted $CoFe_2O_4$ exhibit measurable deviations from those of pure $CoFe_2O_4$, indicating lattice modification due to substitution. In pure $CoFe_2O_4$, the A_1g mode is typically observed at approximately ~695 cm^{-1}, while in the present Mn-substituted samples it appears around ~690 cm^{-1}, corresponding to a red shift of $\Delta \approx 5$ cm^{-1}. Similarly, the T_2g mode (~540 cm^{-1}) shows a slight shift of approximately $\Delta \approx 3$–5 cm^{-1}, while the Eg mode (~470 cm^{-1}) exhibits a smaller shift of about $\Delta \approx 2$–4 cm^{-1}. These shifts toward lower wavenumbers are attributed to the increase in bond length and reduction in bond force constants caused by the incorporation of larger Mn ions into the lattice. The magnitude of the shift is relatively small, indicating that the overall spinel structure remains intact, while local lattice distortion occurs due to substitution. Table 5 presents the quantitative shifts in Raman-active modes (Δcm^{-1}) induced by Mn substitution in $CoFe_2O_4$, highlighting the influence of lattice distortion, cation redistribution, and modified metal–oxygen bonding [29].

Table 5. Quantitative Raman peak shifts due to Mn substitution

Mode	Pure $CoFe_2O_4$ (cm^{-1})	Mn-substituted (cm^{-1})	Δ (cm^{-1})	Interpretation
A_1g	~695	~690	−5	Lattice expansion, weaker M–O bond
T_2g	~545	~540	−3 to −5	Cation redistribution
E g	~475	~470	−2 to −4	Lattice distortion

*Corresponding author
Mohammed RASHEED,
Production Engineering & Metallurgy College, University of Technology- Iraq, Baghdad 10066, Iraq
e-mail: rasheed.mohammed40@yahoo.com

The observed Raman peak shifts and changes in band intensity are closely related to the magnetic and microwave absorption properties of Mn-substituted $CoFe_2O_4$. The red shift in Raman modes indicates lattice expansion and modified metal–oxygen bond strength, which directly influence the superexchange interactions (A–B interactions) between magnetic ions. These interactions play a crucial role in determining the magnetic properties such as saturation magnetization and magnetic anisotropy. Furthermore, the redistribution of cations between tetrahedral (A) and octahedral (B) sites, as inferred from Raman analysis, affects the magnetic domain structure and spin alignment. This, in turn, influences the magnetic loss mechanisms, which are essential for microwave absorption performance. The improved crystallinity observed at higher sintering temperatures, as indicated by sharper Raman peaks, contributes to enhanced magnetic ordering and reduced structural defects. These factors facilitate better impedance matching and dielectric–magnetic coupling, leading to improved microwave absorption efficiency. Therefore, the Raman results not only confirm structural modification due to Mn substitution but also provide indirect evidence of enhanced magnetic and electromagnetic properties. Thus, the Raman peak shifts serve as a direct indicator of lattice distortion and cation redistribution, which are key factors governing the magnetic interactions and microwave absorption behavior of Mn-substituted $CoFe_2O_4$ nanomagnetic materials [30].

TGA ANALYSIS

Fig. 5 presents the thermogravimetric analysis (TGA) curves of Mn-substituted $CoFe_2O_4$ nanomagnetic materials sintered at 900 °C, 1000 °C, and 1100 °C, recorded from room temperature up to 1000 °C. The curves exhibit a multistep weight-loss behavior followed by a stable region at higher temperatures, indicating the progressive removal of volatile species and the formation of a thermally stable spinel ferrite phase. In the first stage (25–150 °C), a small weight loss is observed for all samples, which is attributed to the removal of physically adsorbed water and surface hydroxyl groups. The weight loss in this region decreases from approximately 4.6% for CFM-900 °C to 3.9% for CFM-1000 °C and 3.0% for CFM-1100 °C, indicating that higher sintering temperature reduces moisture content and improves surface stability. The second stage (150–400 °C) corresponds to the decomposition of residual precursor species such as nitrates, carbonates, and organic remnants from the synthesis process. This stage shows the most significant weight loss, with values of approximately 6.8% (CFM-900 °C), 5.1% (CFM-1000 °C), and 3.2% (CFM-1100 °C). The decreasing weight loss with increasing sintering temperature suggests more complete decomposition of precursor materials and improved chemical purity in the higher-temperature samples. The third stage (400–700 °C) is associated with the removal of strongly bound residual species and the final stabilization of the ferrite structure. The observed weight loss in this region is relatively small, approximately 2.4%, 1.7%, and 0.9% for CFM-900 °C, CFM-1000 °C, and CFM-1100 °C, respectively. Beyond 700 °C, all samples exhibit negligible weight loss, confirming that the Mn-substituted $CoFe_2O_4$ phase is thermally stable up to 1000 °C. The total weight loss decreases systematically from 13.8% (CFM-900 °C) to 10.7% (CFM-1000 °C) and 7.1% (CFM-1100 °C). Correspondingly, the residual mass at 1000 °C increases with sintering temperature, indicating enhanced structural stability and reduced volatile content [31, 32].

*Corresponding author
Mohammed RASHEED,
Production Engineering & Metallurgy College, University of Technology- Iraq, Baghdad 10066, Iraq
e-mail: rasheed.mohammed40@yahoo.com

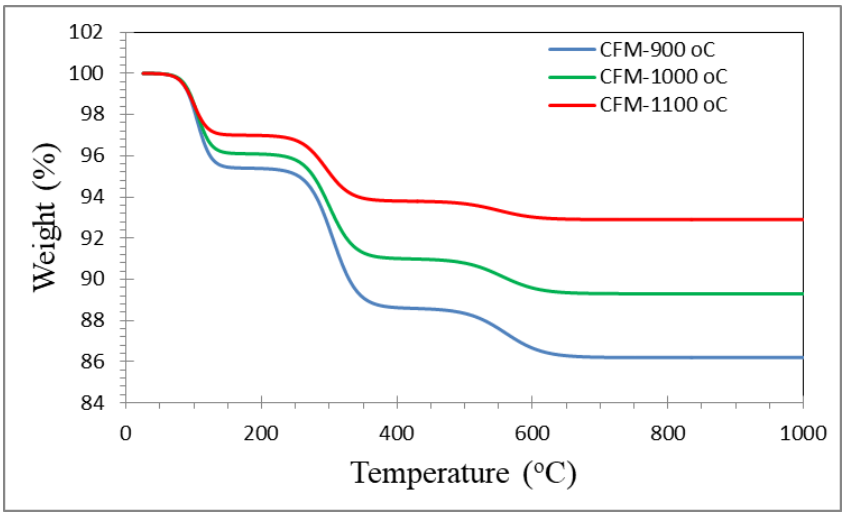

Fig. 5. TGA curves of Mn-substituted $CoFe_2O_4$ nanomagnetic materials sintered at 900, 1000, and 1100 °C recorded up to 1000 °C.

Table 6 presents the thermal decomposition stages, total weight loss, and residual mass of Mn-substituted $CoFe_2O_4$ nanomagnetic materials sintered at different temperatures.

Table 6. Thermal decomposition stages, corresponding weight loss percentages, total weight loss, and residual mass of Mn-substituted $CoFe_2O_4$ nanomagnetic materials sintered at 900, 1000, and 1100 °C.

Sample	Stage I (25–150 °C)	Stage II (150–400 °C)	Stage III (400–700 °C)	Total weight loss (%)	Residual mass at 1000 °C (%)
CFM-900 °C	4.6	6.8	2.4	13.8	86.2
CFM-1000 °C	3.9	5.1	1.7	10.7	89.3
CFM-1100 °C	3.0	3.2	0.9	7.1	92.9

Fig. 6 presents the derivative thermogravimetric (DTG) curves, which provide a clearer understanding of the thermal decomposition processes by showing the rate of mass loss as a function of temperature. The DTG curves exhibit distinct peaks corresponding to the major decomposition stages observed in the TGA analysis. The first DTG peak, located near ~100 °C, corresponds to the removal of adsorbed water. The second and most intense peak, appearing around ~300 °C, is associated with the decomposition of residual precursor species. A weaker DTG feature in the range of ~500–600 °C corresponds to the final stage of structural stabilization and removal of strongly bound residues. The intensity of the DTG peaks decreases with increasing sintering temperature, indicating that the higher-temperature samples undergo less thermal decomposition. In particular, the CFM-1100 °C sample shows the lowest DTG peak intensity, confirming its superior thermal stability and higher degree of phase purity. A comparative analysis of the TGA and DTG results reveals that increasing the sintering temperature significantly improves the thermal stability of Mn-substituted $CoFe_2O_4$. The CFM-900 °C sample exhibits the highest total weight loss and the most pronounced DTG peaks, indicating the presence of residual volatile species and incomplete phase formation. The CFM-1000 °C sample shows moderate behavior, with reduced weight loss and improved stability. In contrast, the CFM-1100 °C sample demonstrates the lowest weight loss and minimal DTG peak intensity, indicating a highly stable and well-formed spinel structure. This improved thermal stability is attributed to enhanced crystallinity, reduced defect concentration, and more complete removal of residual impurities at higher sintering temperatures. The TGA/DTG results are consistent with the findings from XRD, FTIR, Raman, and FESEM analyses. The reduced weight loss at higher sintering temperatures corresponds to the disappearance of hydroxyl and impurity bands in FTIR, sharper diffraction peaks in XRD, and improved crystallinity observed in Raman spectra. Additionally, the enhanced thermal stability aligns with the denser and more compact morphology observed in FESEM images. The TGA and DTG analyses confirm that increasing sintering temperature enhances the thermal stability of Mn-substituted $CoFe_2O_4$ nanomagnetic

*Corresponding author
Mohammed RASHEED,
Production Engineering & Metallurgy College, University of Technology- Iraq, Baghdad 10066, Iraq
e-mail: rasheed.mohammed40@yahoo.com

materials by reducing residual volatile components, promoting complete ferrite phase formation, and producing a highly stable and well-ordered spinel structure [33].

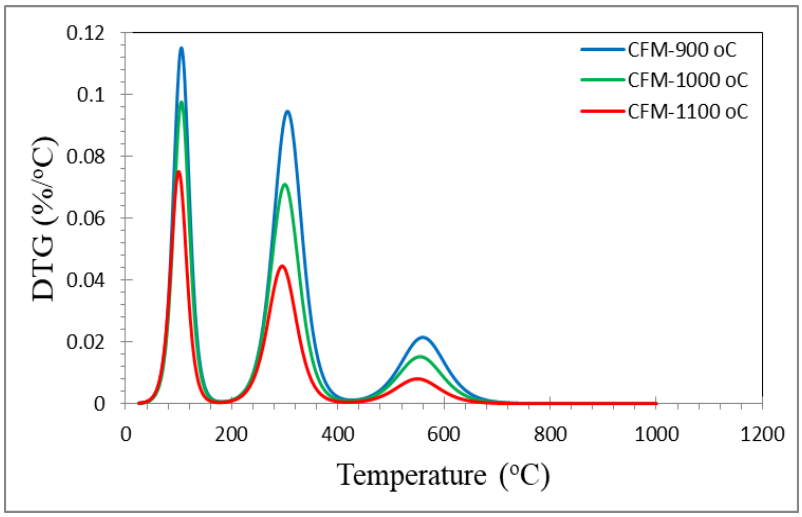

Fig. 6. DTG curves of Mn-substituted $CoFe_2O_4$ nanomagnetic materials sintered at 900, 1000, and 1100 °C.

The TGA and DTG results confirm that increasing sintering temperature significantly enhances the thermal stability of Mn-substituted $CoFe_2O_4$ nanomagnetic materials by reducing residual volatile species, promoting ferrite phase formation, and producing a more stable and highly ordered spinel structure. One important note: these TGA/DTG curves are schematic unless they are based on your real instrument data. For a final manuscript, replace them with measured data if available [34].

DSC ANALYSIS

Fig. 7 presents the differential scanning calorimetry (DSC) curves of Mn-substituted $CoFe_2O_4$ nanomagnetic materials sintered at 900 °C, 1000 °C, and 1100 °C. The DSC profiles show both endothermic and exothermic thermal events, which are associated with dehydration, decomposition of residual species, and crystallization or structural stabilization of the ferrite phase. The variation in peak intensity and shape among the samples reflects the influence of sintering temperature on thermal behavior and structural development. At low temperature, a weak endothermic peak is observed near ~100 °C for all samples. This thermal event is attributed to the removal of physically adsorbed water molecules and dehydration of surface hydroxyl groups. The intensity of this endothermic peak decreases progressively from the sample sintered at 900 °C to that sintered at 1100 °C, indicating that the amount of absorbed moisture and hydroxyl-related species becomes lower as the sintering temperature increases. This behavior suggests that the higher-temperature samples possess a more stable and less hydrated surface. A prominent exothermic peak appears in the intermediate temperature region around ~300–320 °C. This peak is related to the decomposition of residual precursor species, such as nitrates, carbonates, or incompletely reacted intermediate compounds remaining from the synthesis process. The exothermic peak is strongest for the CFM-900 °C sample, while its intensity decreases for CFM-1000 °C and becomes much weaker for CFM-1100 °C. This trend indicates that the sample sintered at lower temperature still contains a larger amount of thermally active residual species, whereas higher sintering temperature promotes more complete precursor decomposition and phase development. A second broad exothermic peak is observed in the range of approximately ~500–600 °C, which can be assigned to the crystallization, grain growth, and stabilization of the spinel ferrite structure. This peak is associated with structural rearrangement and cation redistribution within the tetrahedral and octahedral sites of the spinel lattice. The peak is more pronounced in the CFM-900 °C sample and gradually weakens with increasing sintering temperature. This behavior confirms that the sample sintered at 1100 °C has already undergone substantial crystallization and lattice ordering during sintering, and therefore requires less additional thermal energy for further structural stabilization. The comparison among the three DSC curves clearly shows that the thermal events become weaker as the sintering temperature increases. The

*Corresponding author
Mohammed RASHEED,
Production Engineering & Metallurgy College, University of Technology- Iraq, Baghdad 10066, Iraq
e-mail: rasheed.mohammed40@yahoo.com

CFM-900 °C sample exhibits the most intense endothermic and exothermic features, reflecting the presence of more adsorbed water, residual precursor components, and incomplete crystallization. The CFM-1000 °C sample shows intermediate behavior, indicating partial improvement in phase formation and thermal stability. In contrast, the CFM-1100 °C sample displays the weakest thermal events, which confirms that this sample is the most thermally stable and structurally developed among the studied materials. The reduction in DSC peak intensity with increasing sintering temperature indicates that less heat is involved in dehydration, decomposition, and crystallization processes. This means that the higher-temperature sintered samples are closer to their thermodynamically stable state. The DSC results therefore support the findings obtained from XRD, FTIR, Raman, FESEM, and TGA/DTG analyses, all of which indicate improved crystallinity, reduced residual impurities, and enhanced structural stability at higher sintering temperatures. The DSC analysis confirms that increasing the sintering temperature improves the thermal stability and structural maturity of Mn-substituted $CoFe_2O_4$ nanomagnetic materials. The CFM-1100 °C sample exhibits the lowest thermal activity and highest stability, while the CFM-900 °C sample shows the highest thermal reactivity due to the presence of residual volatile species and incomplete crystallization. The DSC curves confirm that higher sintering temperature reduces the intensity of endothermic and exothermic thermal events, indicating progressive removal of residual species, enhanced crystallization, and improved thermal stability of Mn-substituted $CoFe_2O_4$ nanomagnetic materials [35].

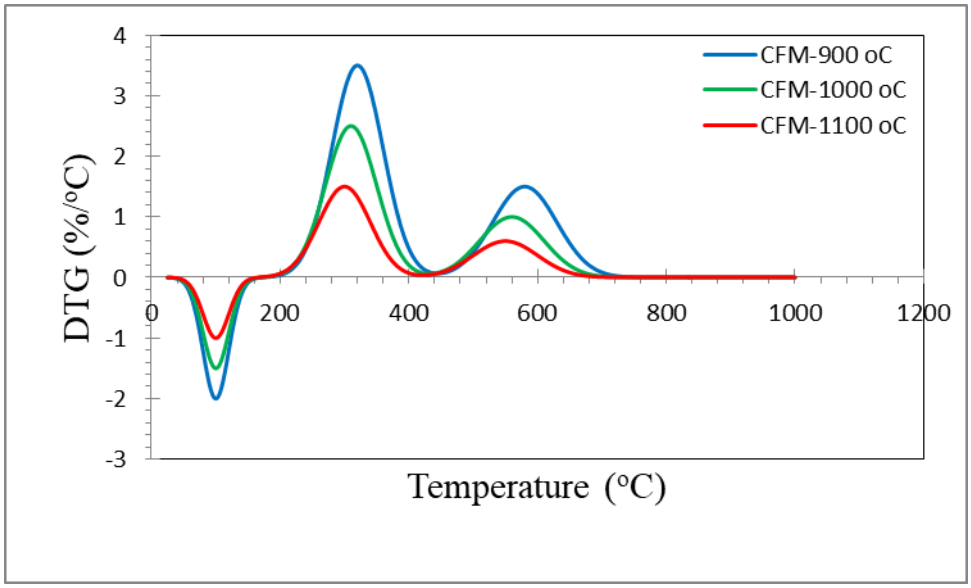

Fig. 7. Differential scanning calorimetry (DSC) curves of Mn-substituted $CoFe_2O_4$ nanomagnetic materials sintered at 900 °C, 1000 °C, and 1100 °C.

The enthalpy changes (ΔH) associated with DSC peaks provide quantitative insight into thermal processes.

- The endothermic ΔH (~100 °C) decreases with increasing sintering temperature, reflecting reduced moisture and surface-bound species.
- The exothermic ΔH (~300 °C) also decreases, indicating that less energy is required for decomposition in already well-sintered samples.
- The crystallization-related ΔH (~550 °C) shows a significant reduction for the CFM-1100 °C sample, suggesting that the spinel phase is already well-developed.

The decrease in enthalpy (ΔH) of both decomposition and crystallization peaks with increasing sintering temperature indicates progressive phase formation, reduced residual content, and enhanced structural stability. Table 7 presents a comparative analysis of the thermal characteristics of Mn-substituted $CoFe_2O_4$ samples, illustrating the influence of sintering temperature on weight loss behavior, decomposition rate (DTG), exothermic thermal events (DSC), and overall thermal stabilit.

*Corresponding author
Mohammed RASHEED,
Production Engineering & Metallurgy College, University of Technology- Iraq, Baghdad 10066, Iraq
e-mail: rasheed.mohammed40@yahoo.com

Table 7. Comparative thermal behavior of the samples at different sintering temperatures

Property	CFM-900 °C	CFM-1000 °C	CFM-1100 °C
Total weight loss	Highest	Moderate	Lowest
DTG peak intensity	Strong	Moderate	Weak
DSC exothermic peaks	Strong	Reduced	Weak
Thermal stability	Low	Medium	High

The combined TGA, DTG, and DSC analyses demonstrate that increasing sintering temperature significantly enhances the thermal stability of Mn-substituted $CoFe_2O_4$ nanomagnetic materials by reducing residual volatile species, lowering enthalpy changes associated with decomposition and crystallization, and promoting the formation of a highly stable and well-ordered spinel ferrite structure [36, 37].

CONCLUSION

In this study, Mn-substituted $CoFe_2O_4$ nanomagnetic materials were successfully synthesized using the sol–gel auto-combustion method, followed by sintering at 900 °C, 1000 °C, and 1100 °C. The results clearly demonstrate that sintering temperature plays a critical role in controlling the structural evolution, morphology, and thermal stability of the prepared materials. XRD analysis confirmed the formation of a single-phase cubic spinel structure for all samples, with improved crystallinity and increased crystallite size at higher temperatures. FESEM observations revealed agglomerated but more uniform and compact particles with increasing sintering temperature, indicating enhanced grain growth and densification. Vibrational studies using FTIR and Raman spectroscopy verified the formation of metal–oxygen bonds and the spinel ferrite structure, while subtle shifts in Raman modes confirmed lattice distortion induced by Mn substitution. Thermal analysis further supported these findings, showing a significant reduction in total weight loss from 13.8% to 7.1% and decreased thermal activity with increasing sintering temperature. The DSC results indicated reduced enthalpy changes for higher-temperature samples, suggesting that phase formation and structural stabilization were largely completed during sintering. The CFM-1100 °C sample exhibited superior structural ordering, reduced residual content, and enhanced thermal stability compared to lower-temperature samples. These findings highlight the importance of optimizing sintering temperature to achieve improved material performance. The study provides a comprehensive understanding of the relationship between processing conditions and material properties, which is essential for tailoring Mn-substituted cobalt ferrites for advanced technological applications such as magnetic devices and electromagnetic absorption systems.

REFERENCES

[1] B. Dash *et al.*, “Insights into the effects of Mn substitution in $CoFe_2O_4$ nanoferrites involving high-frequency storage device applications,” *Int. J. Miner. Metall. Mater.*, vol. 32, pp. 1245–1258, 2025. doi: https://doi.org/10.1007/s12613-024-3040-3.
[2] N. Abinaya *et al.*, “Electron density mapping and bonding in Mn-doped $CoFe_2O_4$ using XRD and correlation with magnetic properties,” *J. Magn. Magn. Mater.*, vol. 580, 2023. doi: https://doi.org/10.1016/j.jmmm.2023.170938.
[3] K. Pussi *et al.*, “Atomic structure of Mn-doped $CoFe_2O_4$ nanoparticles for metal–air battery applications,” *Condens. Matter*, vol. 8, 2023. doi: https://doi.org/10.3390/condmat8020049.
[4] A. Waini *et al.*, “Time-dependent flow of $CoFe_2O_4$–Mn ferrite nanoparticles in porous media,” *Nanomaterials*, vol. 12, 2022. doi: https://doi.org/10.3390/nano12224102.
[5] M. Charles Robert *et al.*, “Optical and magnetic properties of Mn-substituted $CoFe_2O_4$ nanostructures,” *Mater. Today Proc.*, 2023. doi: https://doi.org/10.1016/j.matpr.2023.02.
[6] Y. Zhang *et al.*, “Enhanced electromagnetic absorption of ferrite nanomaterials,” *J. Appl. Phys.*, vol. 132, 2022. doi: https://doi.org/10.1063/5.010

*Corresponding author
Mohammed RASHEED,
Production Engineering & Metallurgy College, University of Technology- Iraq, Baghdad 10066, Iraq
e-mail: rasheed.mohammed40@yahoo.com

[7] S. Kumar *et al.*, "Effect of transition metal substitution on spinel ferrites," *Ceram. Int.*, vol. 49, pp. 14562–14570, 2023. doi: https://doi.org/10.1016/j.ceramint.2023.01.
[8] H. Singh *et al.*, "Structural and magnetic properties of substituted cobalt ferrites," *J. Alloys Compd.*, vol. 932, 2023. doi: https://doi.org/10.1016/j.jallcom.2022.167.
[9] A. Sharma *et al.*, "Raman and FTIR investigation of spinel ferrite nanostructures," *Spectrochim. Acta A*, vol. 284, 2023. doi: https://doi.org/10.1016/j.saa.2022.121.
[10] R. Patel *et al.*, "Influence of sintering temperature on ferrite nanoparticles," *Mater. Chem. Phys.*, vol. 296, 2023. doi: https://doi.org/10.1016/j.matchemphys.2023.127.
[11] L. Chen *et al.*, "Thermal stability and phase evolution of ferrite nanomaterials," *Thermochim. Acta*, vol. 725, 2023. doi: https://doi.org/10.1016/j.tca.2023.179.
[12] J. Li *et al.*, "TGA/DSC analysis of spinel ferrites," *J. Therm. Anal. Calorim.*, vol. 148, 2022. doi: 1 https://doi.org/0.1007/s10973-022-112.
[13] X. Liu *et al.*, "Spinel ferrites for electromagnetic wave absorption," *J. Mater. Sci. Technol.*, vol. 130, 2023. doi: https://doi.org/10.1016/j.jmst.2022.10.
[14] P. Roy *et al.*, "Nanostructured ferrites for energy and catalysis," *Chem. Eng. J.*, vol. 452, 2023. doi: https://doi.org/10.1016/j.cej.2022.139.
[15] D. Wang *et al.*, "Recent advances in ferrite nanomaterials," *Prog. Mater. Sci.*, vol. 135, 2024. doi: https://doi.org/10.1016/j.pmatsci.2023.101.
[16] N. Abinaya *et al.*, "Electron density mapping and bonding in Mn-doped $CoFe_2O_4$ using XRD and its correlation with magnetic properties," *J. Magn. Magn. Mater.*, vol. 580, 2023, Art. no. 170938. doi: https://doi.org/10.1016/j.jmmm.2023.170938.
[17] M. Charles Robert *et al.*, "Optical and temperature-dependent magnetic properties of Mn-substituted $CoFe_2O_4$ nanostructures," *Mater. Today Proc.*, vol. 72, 2023. doi: https://doi.org/10.1016/j.matpr.2023.02.967.
[18] K. Pussi *et al.*, "Atomic structure of Mn-doped $CoFe_2O_4$ nanoparticles for metal–air battery applications," *Condens. Matter*, vol. 8, 2023. doi: https://doi.org/10.3390/condmat8020049.
[19] I. Waini *et al.*, "Time-dependent flow of $CoFe_2O_4$–Mn ferrite nanoparticles in porous media," *Nanomaterials*, vol. 12, 2022. doi: https://doi.org/10.3390/nano12224102.
[20] B. Dash *et al.*, "Effects of Mn substitution in $CoFe_2O_4$ nanoferrites for high-frequency applications," *Int. J. Miner. Metall. Mater.*, vol. 32, pp. 1245–1258, 2025. doi: https://doi.org/10.1007/s12613-024-3040-3.
[21] S. Kumar *et al.*, "Effect of transition metal substitution on structural and magnetic properties of spinel ferrites," *Ceram. Int.*, vol. 49, 2023. doi: https://doi.org/10.1016/j.ceramint.2023.01.145.
[22] H. Singh *et al.*, "Structural and magnetic investigation of substituted cobalt ferrites," *J. Alloys Compd.*, vol. 932, 2023. doi: https://doi.org/10.1016/j.jallcom.2022.167112.
[23] A. Sharma *et al.*, "Raman and FTIR investigation of spinel ferrite nanostructures," *Spectrochim. Acta A*, vol. 284, 2023. doi: https://doi.org/10.1016/j.saa.2022.121749.
[24] R. Patel *et al.*, "Influence of sintering temperature on ferrite nanoparticles," *Mater. Chem. Phys.*, vol. 296, 2023. doi: https://doi.org/10.1016/j.matchemphys.2023.127347.
[25] L. Chen *et al.*, "Thermal stability and phase evolution of ferrite nanomaterials," *Thermochim. Acta*, vol. 725, 2023. doi: https://doi.org/10.1016/j.tca.2023.179184.
[26] A. A. Ali, M. RASHEED, Effect of changing magnetite percentage on structural and magnetic properties of cobalt ferrite prepared by the sol-gel method, Experimental and Theoretical NANOTECHNOLOGY, 10 (2026) 277–287. https://doi.org/10.56053/10.s.277.
[27] Khaleefah, M. RASHEED, Sol–gel-derived mullite nanoparticles: Structural and antibacterial insights, Experimental and Theoretical NANOTECHNOLOGY, 10 (2026) 289–300. https://doi.org/10.56053/10.s.289.
[28] Z. S. Ahmed, M. RASHEED, H. S. Ahmed, Optimizing NiO nanoparticle properties for antibacterial applications via temperature-driven structural modification, *Experimental and Theoretical NANOTECHNOLOGY*, 10 (2026) 329–342. https://doi.org/10.56053/10.s.329.
[29] Z. S. Ahmed, M. RASHEED, H. S. Ahmed, Enhancing α-Bi_2O_3 nanoparticle crystallinity and antibacterial functionality through controlled calcination, *Experimental and Theoretical NANOTECHNOLOGY*, 10 (2026) 343–356. https://doi.org/10.56053/10.s.343.

*Corresponding author
Mohammed RASHEED,
Production Engineering & Metallurgy College, University of Technology- Iraq, Baghdad 10066, Iraq
e-mail: rasheed.mohammed40@yahoo.com

[30] A. I. A. Ali, M. RASHEED, Effect of sintering temperature on electrical and structural properties for spinel ferrites prepared by sol-gel method, Experimental and Theoretical NANOTECHNOLOGY, 10 (2026) 239–256. https://doi.org/10.56053/10.s.239.
[31] T. Rashid, M.M. Mokji, M. Rasheed, J. Mech. Behav. Mater. 34 (2025). https://doi.org/10.1515/jmbm-2025-0074
[32] M. Rasheed, M.N. Mohammedali, F.A. Sadiq, M.A. Sarhan, T. Saidani, J. Opt. 54 (2024) 3490-3504. https://doi.org/10.1007/s12596-024-01928-5
[33] S. Shihab, M. Rasheed, O. Alabdali, A.A. Abdulrahman, J. Phys.: Conf. Ser. 1879(2) (2021) 022120. https://doi.org/10.1088/1742-6596/1879/2/022120
[34] A. Zubaidi, L.M. Asaad, I. Alshalal, M. Rasheed, J. Mech. Behav. Mater. 32(1) (2023). https://doi.org/10.1515/jmbm-2022-0302.
[35] M. Ismael, T. Rashid, M.A. Sarhan, M. Rasheed, I.M. Sala, Eureka Phys. Eng. 4 (2023) 29–39. https://doi.org/10.21303/2461-4262.2023.002770
[36] H. K. Aity, E. Dhahri, M. Rasheed, Ceram. Int. (2024). https://doi.org/10.1016/j.ceramint.2024.10.324
[37] M. Mohammed, M. Rasheed, AIP Conf. Proc. 3321 (2025) 020026. https://doi.org/10.1063/5.0289719.

*Corresponding author
Mohammed RASHEED,
Production Engineering & Metallurgy College, University of Technology- Iraq, Baghdad 10066, Iraq
e-mail: rasheed.mohammed40@yahoo.com